

NARRATIVE REVIEW

Open Access

Musculoskeletal MRI at 7 T: do we need more or is it more than enough?



Giacomo Aringhieri^{1*} , Virna Zampa² and Michela Tosetti³

Abstract

Ultra-high field magnetic resonance imaging (UHF-MRI) provides important diagnostic improvements in musculoskeletal imaging. The higher signal-to-noise ratio leads to higher spatial and temporal resolution which results in improved anatomic detail and higher diagnostic confidence. Several methods, such as T2, T2*, T1rho mapping, delayed gadolinium-enhanced, diffusion, chemical exchange saturation transfer, and magnetisation transfer techniques, permit a better tissue characterisation. Furthermore, UHF-MRI enables *in vivo* measurements by low- γ nuclei (^{23}Na , ^{31}P , ^{13}C , and ^{39}K) and the evaluation of different tissue metabolic pathways. European Union and Food and Drug Administration approvals for clinical imaging at UHF have been the first step towards a more routinely use of this technology, but some drawbacks are still present limiting its widespread clinical application. This review aims to provide a clinically oriented overview about the application of UHF-MRI in the different anatomical districts and tissues of musculoskeletal system and its pros and cons. Further studies are needed to consolidate the added value of the use of UHF-MRI in the routine clinical practice and promising efforts in technology development are already in progress.

Keywords: Cartilage (articular), Magnetic resonance imaging, Magnetic resonance spectroscopy, Musculoskeletal system, Ultra-high field magnetic resonance imaging

Key points

- Ultra-high field magnetic resonance imaging (UHF-MRI) provides higher spatiotemporal and spectral resolution compared to 1.5-T or 3-T MRI.
- Better morphologic, biochemical, and functional details of musculoskeletal tissues are achievable using 7-T magnets.
- UHF-MRI improves the diagnostic accuracy, in particular articular cartilage.
- Current and potential future musculoskeletal applications of UHF-MRI are rising.
- Many efforts are in progress to overcome the limitations for clinical application.

Background

Ultra-high field (UHF) magnetic resonance imaging (MRI), in particular 7-T MRI, has a well-demonstrated role in musculoskeletal (MSK) imaging. In comparison with lower magnetic fields, UHF-MRI provides an increased signal-to-noise ratio (SNR) that can selectively increase spatial and/or temporal resolution. UHF-MRI also provides improved spectral resolution and sensitivity for X-nucleus imaging, *i.e.*, ^{23}Na , ^{31}P , ^{13}C , and ^{39}K [1]. UHF-MRI has been applied in many MSK fields, in particular for the study of cartilage but also of menisci, bone, ligaments, tendons, and skeletal muscles.

Recently, clinical interest in UHF-MRI is progressively rising, supported by the European Union and by the Food and Drug Administration (FDA) approvals for clinical 7-T MRI in 2017 [2, 3]. Most of MSK UHF-MRI reviews are mainly focused on techniques and technologies. This manuscript intends to provide a clinically oriented overview, following the pathway from the experimental settings to clinical applications, allowing

* Correspondence: giacomo.aringhieri@unipi.it

This is the second article of a thematic series entitled "Advances in MSK imaging and imaging-guided interventions" (Guest Editors Prof. Luca Maria Sconfienza (Milan/IT) and Prof. Franz Kainberger (Vienna/AT)).

¹Department of Translational Research and New Technologies in Medicine and Surgery, University of Pisa, Via Risorgimento, 36 Pisa, Italy
Full list of author information is available at the end of the article

the readers to more easily identify the UHF-MRI novelties for each MSK district or structure and to explore current and potential clinical applications.

Cartilage

The main MSK field of application is cartilage, mostly regarding morphological study, ultrastructural composition, volumetric segmentation, and biochemical evaluation. The main clinical topic in cartilage studies is osteoarthritis (OA), aimed at detecting preclinical degenerative changes in ageing joints.

Morphological imaging

The increased spatial resolution permits to evaluate microscopic morphological changes before the onset of OA symptoms, taking advantage also of shortened protocols thanks to the use of parallel imaging [4] and three-dimensional (3D) acquisitions [5]. Jin et al. [6] obtained high spatial resolution images of knee and ankle joints with an open eight-channel parallel transmission coil reaching an in-plane resolution of 0.3 mm with turbo spin-echo sequences and of 0.47 mm with isotropic dual-echo steady state acquisitions. Additionally, the U-shape coil permitted to dynamically scan the joints both in flexion and extension. Similar results were also achieved by many authors with different coils and sequences, as summarised in Table 1 [6–10].

However, all the authors underline the mandatory preliminary work on sequences optimisation and the need for dedicated coils, often not commercially available. Poor fat saturation, extensive artefacts and increased specific absorption rate (SAR) may occur during clinical protocols optimisation at UHF [8]. However, MRI technological advances will overcome these technical limitations, especially with the introduction of dedicated, multichannel, transmit-receive coils [11].

Knee Welsch et al. demonstrated the superiority of 7-T over 3-T magnets for quantitative and qualitative cartilage evaluation, in terms of higher spatial resolution, higher contrast-to-noise ratio (CNR) and potentially

reduced acquisition time [12]. Aringhieri et al. [13] showed a comparison of the overall image quality, meant as higher spatial resolution, obtained scanning the same knee of the same subject at 1.5 T, 3 T, and 7 T (Fig. 1): the optimised spatial and contrast resolution led to better cartilage depiction and boundary partial-volume artefacts reduction, enabling a more precise estimation of cartilage volumes. Springer et al. [11] analysed the diagnostic confidence comparing for the first time similar clinical protocol at 3 T and 7 T in 40 patients with knee pain. Despite a certain image quality reduction due to chemical shift artefacts, they found an improvement in overall diagnostic potential at 7 T showing an enhanced detection of subtle lesions thanks to the higher SNR and resolution.

Hip Theyshon et al. [10] compared hip joints MRI at 3 T and 7 T, concluding that 7-T MRI showed slight advantages in cartilage defects and fluid detection with clinical performance comparable to 3-T magnets. However, 7-T MRI was more prone to artefacts due to B_1 inhomogeneities, radiofrequency (RF) penetration depth and susceptibility effects around periarticular calcifications. Even magnetic fields higher than 7 T have been explored for hip MRI, as demonstrated by He et al. [14] reporting a detailed depiction of fine structures with a 0.7-mm isotropic voxel and excellent contrast at 10.5 T. Thanks to RF management strategies developed for 7-T magnets and phase shimming techniques, they obtained suitable bilateral hip images at 10.5 T with even better results when unilateral imaging was performed.

Ankle Comparing ankle MRI at 3 T and 7 T, a significant increase in SNR at 7 T using a 3D gradient-echo (GRE) and two-dimensional (2D) turbo spin-echo (TSE) sequences was demonstrated, while a decrease on 2D spin-echo sequences was observed. An increased CNR was found for all the sequences except for cartilage-to-muscle contrast on the 3D GRE sequence [15]. Compared to 1.5-T MRI, 7-T MRI provided an improved depiction of the ankle anatomy and a better detection of

Table 1 Spatial resolution obtained at 7-T

Authors [reference]	Year	Sequence type	Technique	Joint	In-plane resolution (mm)	Slice thickness (mm)
Regatte and Schweitzer [7]	2007	FLASH	3D	Knee	0.25 × 0.25	1.00
Stahl et al. [8]	2009	FIESTA-C	3D	Knee	0.25 × 0.25	1.00
Behr et al. [9]	2009	GRE	2D	Wrist, Hand	0.16 × 0.16	1.50
Behr et al. [9]	2009	GRE	3D	Wrist, Hand	0.27 × 0.27	0.30
Theyshon et al. [10]	2013	DESS	2D	Hip	0.38 × 0.38	0.76
Jin et al. [6]	2018	TSE	2D	Knee, Ankle	0.30 × 0.30	2.50
Jin et al. [6]	2018	DESS	3D	Knee, Ankle	0.47 × 0.47	0.47

FLASH Fast low angle shot, FIESTA-C Fast imaging employing steady-state acquisition with coherence interference, GRE Gradient-echo, DESS Double steady state, TSE Turbo spin-echo

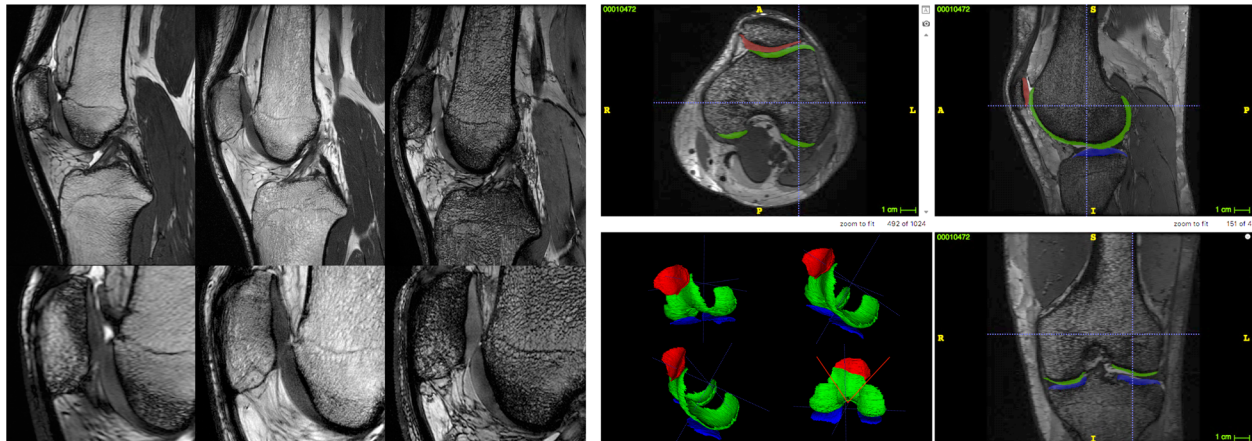


Fig. 1 At the top left, the comparison of the same knee of the same healthy volunteer acquired with fast imaging employing steady-state acquisition with coherence interference (FIESTA-C) at 1.5-T, 3-T, and 7-T (from left to right), showing the improved spatial and contrast resolution for cartilage visualisation. At the bottom left, a detail of the comparison of the femoral-patellar compartment at 1.5-T, 3-T, and 7-T is displayed (from left to right). On the right, an example of semiautomatic segmentation of the different cartilage compartments of the knee is depicted with multiplanar reformation and corresponding volume rendering of the segmented cartilage (red, patellar cartilage; green, femoral cartilage; blue, tibial cartilage). Images were acquired at the University Hospital of Cisanello, Pisa, Italy (1.5-T and 3-T) and at the Imago7 Foundation, Pisa, Italy (7-T). Adapted with permission from Aringhieri et al, *Clin Exp Rheumatol* 2018. Segmentations were performed with ITK-SNAP (<http://www.itksnap.org/pmwiki/pmwiki.php>)

cartilage defects and fluids, despite the usage of a non-dedicated coil. Limitations were the lower efficiency of fat saturation and reduced body coverage using TSE sequences, due to SAR limitations [16].

Wrist and hand Behr et al. [9] demonstrated the superiority of 7-T over 1.5-T MRI with a better depiction of subtle anatomical details not only for cartilage but also for nerves, muscles, tendons, ligaments, pulleys, and blood vessels, especially at when studying the fingers. In particular, time-of-flight sequences resulted in a lower background signal with higher CNR, permitting detailed digital arteries visualisation, exploiting the increased T1 of tissues at 7 T. Nowadays, no studies on clinical applications of UHF-MRI in wrist and hand have been published, yet.

Shoulder Lazik-Palm et al. [17] first demonstrated the feasibility of shoulder clinical protocol acquisition at 7 T with diagnostic image quality. Compared to 1.5-T MRI, higher contrast and spatial resolution obtained at 7 T led to a better image quality and morphological assessment of alterations of the articular structures, including cartilage. Nevertheless, the diagnostic performance of 7-T MRI did not result superior to the results of 3-T MRI reported in the literature [17].

Compositional imaging: T2 mapping

The most used technique for cartilage evaluation is T2 quantitative analysis, mostly obtained as T2 mapping. Cartilage T2 depends on different extracellular matrix

properties, such as tissue anisotropy, water content, collagen concentration, and integrity, while it is insensitive to proteoglycan content. Despite the decreased T2 values at UHF, many studies have been performed at 7 T providing an optimised *in vivo* representation of zonal stratification of cartilage, useful to depict early signs of OA first occurring in the superficial layer [18, 19].

The most used T2 mapping technique for cartilage is a multi-echo spin-echo (MESE) acquisition, which however requires long acquisition time and also implies increased SAR, induced by repeated refocusing RF pulses. Other techniques have been tested for T2 mapping, such as multiple steady state free precession-based sequences, which however are sensitive to B₁ inhomogeneities and do not always provide an accurate and reliable T2 quantification [20]. In 2014, Heule et al. [20] introduced a novel technique, named triple echo steady state (TESS), able to acquire simultaneously T1 and T2 with no influence of B₁ inhomogeneities and of T1 on T2, and *vice versa*. Consistently with MESE results, 3D-TESS was able to detect damaged cartilage as foci of increased T2, with a reduced scan time, insensitive to and B₀ and B₁ inhomogeneities. Examples of the use of this technique are given in Figs. 2 and 3.

Notably, TESS systematically provided lower cartilage T2 values compared to MESE. The overestimation of T2 values obtained with MESE technique was assumed to be related to the stimulated echo contamination due to imperfect refocusing pulses in MESE acquisitions [21, 22]. In Table 2, a summary of the mean T2 values obtained for the cartilage are displayed, showing the

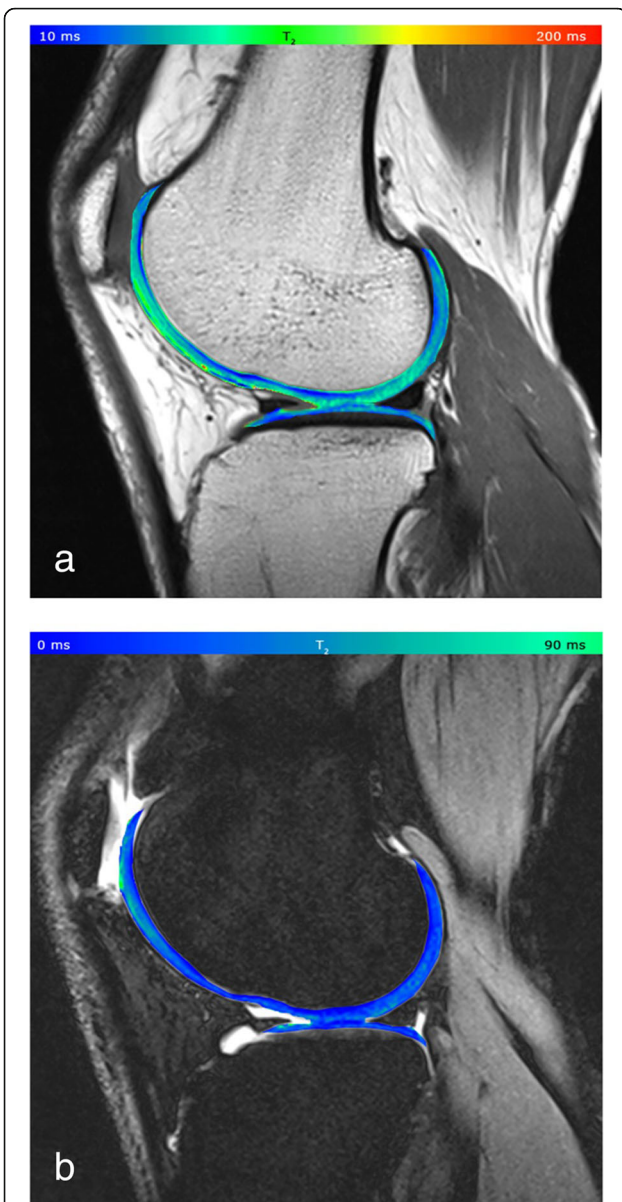


Fig. 2 **a** Cartilage T2 map acquired with a Carr-Purcell-Meiboom-Gill (CPMG) multi-echo spin-echo (MESE) sequence, pseudo-colour-coded and overlaid on a morphological T2-weighted image from a 32-year-old healthy volunteer (echo time 11.9 ms). **b** Cartilage T2 map acquired with a three-dimensional triple echo steady state, pseudo-colour-coded and overlaid on the second acquired image (F_0 , the lowest order steady state free precession—free induction decay mode acquired in the repetition time). The typical zonal stratification of cartilage is observable with both techniques. However, the CPMG sequence provides apparently higher dynamic contrast of T2 values with better depiction of cartilaginous layers. Reprinted with permission from: Juras et al., *Eur Radiol* 2016 (reference [21])

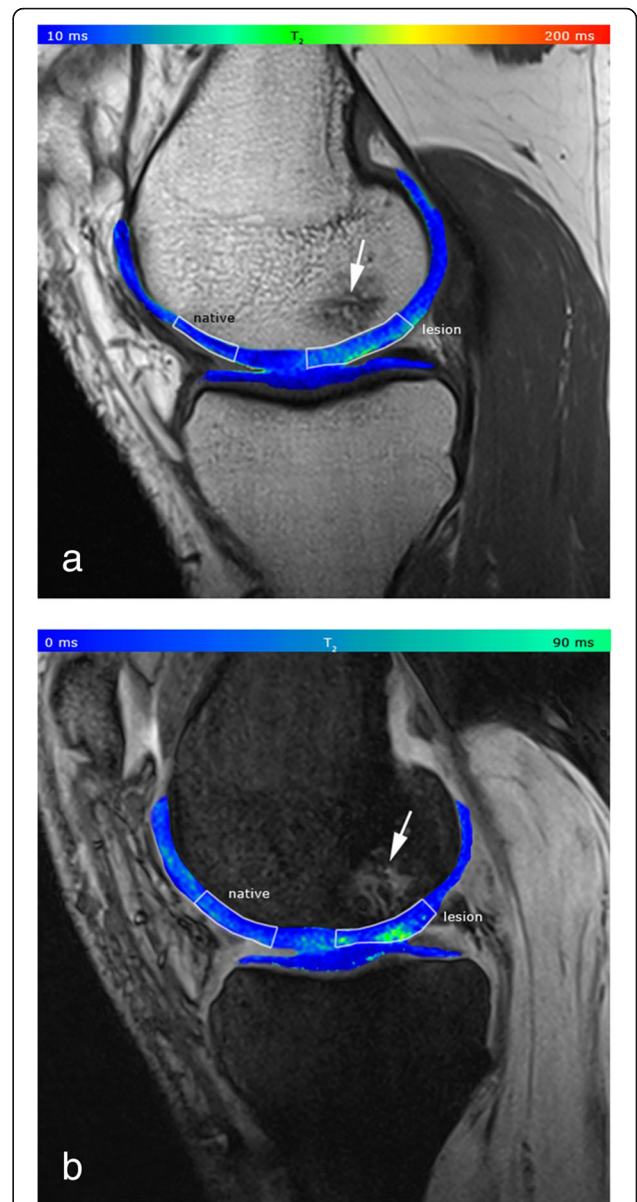


Fig. 3 **a** T2 map acquired with Carr-Purcell-Meiboom-Gill (CPMG) multi-echo spin-echo (MESE) sequence, pseudo-colour-coded and overlaid on a morphological image of a 41-year-old patient with Pridie drilling on the medial femoral condyle (echo time 11.9 ms). The ratio between the native and lesion cartilage T2s was 0.81. **b** T2 map acquired with a three-dimensional triple-echo steady state (3D-TESS) sequence, pseudo-colour-coded and overlaid on the second acquired image (F_0 , the lowest order steady state free precession—free induction decay mode acquired in the repetition time). The ratio between the native and lesion cartilage T2s was 0.83. Focal increase in T2 values is observable with both techniques. Bone oedema is also present (arrow). The dynamic range of the CPMG MESE T2 map is higher compared to that of the 3D-TESS T2 map: the lesion appears to be more diffuse, although the ratios between native and lesion cartilage T2s are comparable. Reprinted with permission from: Juras et al., *Eur Radiol* 2016 (reference [21])

Table 2 Reference T2 values of cartilage in healthy subjects

Authors [reference]	Year	Number of subjects	Age range (years)	Age (years) mean \pm SD	Technique	Joint	T2 values range (ms)	T2 values (ms) mean \pm SD
Welsch et al. [23]	2011	17	n.a.	25.8 \pm 5.7	MESE	Knee	n.a.	41.8 \pm 5.5
Domayer et al. [24]	2011	10	n.a.	30.2 \pm 6.1	MESE	Ankle	n.a.	30.1 \pm 4.2
Lazik et al. [25]	2016	11	21–46	n.a.	MESE	Hip	40.7–44.5	n.a.
Kraff et al. [22]	2016	8	21–39	n.a.	TESS	Hip	19.1–22.6	n.a.
Kraff et al. [22]	2016	8	21–39	n.a.	MESE	Hip	41.1–46.2	n.a.
Juras et al. [26]	2016	10	n.a.	31 \pm 9	TESS	Knee	n.a.	23.5 \pm 3.7
Juras et al. [26]	2016	10	n.a.	31 \pm 9	TESS	Ankle	n.a.	18.8 \pm 2.6

Reference T2 values of the normal cartilage acquired with different techniques in different joints. As reported by Juras et al. [26], in addition to differences in cartilage structure and signal within the same anatomical district, T2 differences are present between different joints, reflecting the different structural composition (Source: Juras et al., *Eur J Radiol* 2016 - reference [26]). *MESE* Multi-echo spin-echo sequence, *n.a.* Not available, *SD* Standard deviation, *TESS* Triple-echo steady state

variations between different anatomical districts and different T2 mapping techniques [26]. When quantitative maps will be included in the clinical routine, it could be useful to perform different techniques during the same examination, including contrast-enhanced sequences. Indeed, relevant effects of gadolinium on post-contrast T2 or T2* mapping have been excluded [27].

Knee Welsch et al. [28] first demonstrated significantly increased T2 values at 7 T, from the deep to the superficial layer of the cartilage, in all the knee compartments, reflecting the different orientation of the collagen fibres: perpendicular to the subchondral bone in the deep zone and parallel to the chondral surface in the superficial zone, as previously demonstrated by Smith et al. [29]. Compared to 3 T, at 7 T a higher CNR was observed and, despite the absolute T2 reduction, a zonal differentiation was still detectable albeit less pronounced [23]. Post-surgical UHF T2 mapping showed significant increased T2 in cartilage repair tissues compared to native cartilage with no significant difference between superficial and deep layers [30, 31]. Among the different biochemical features, only T2 values had significant correlation with the clinical outcome [31]. Wyatt et al. [32] analysed T2 values obtained with 3D magnetisation-prepared angle-modulated partitioned k-space acquisition in healthy volunteers and patients with OA comparing 3-T with 7-T MRI. T2 mapping at 7 T allowed to detect degenerate cartilage in the knee with results comparable to 3-T MRI. Indeed, 7-T MRI provided more significant differences in T2 values between healthy and degenerate cartilage compared to 3 T.

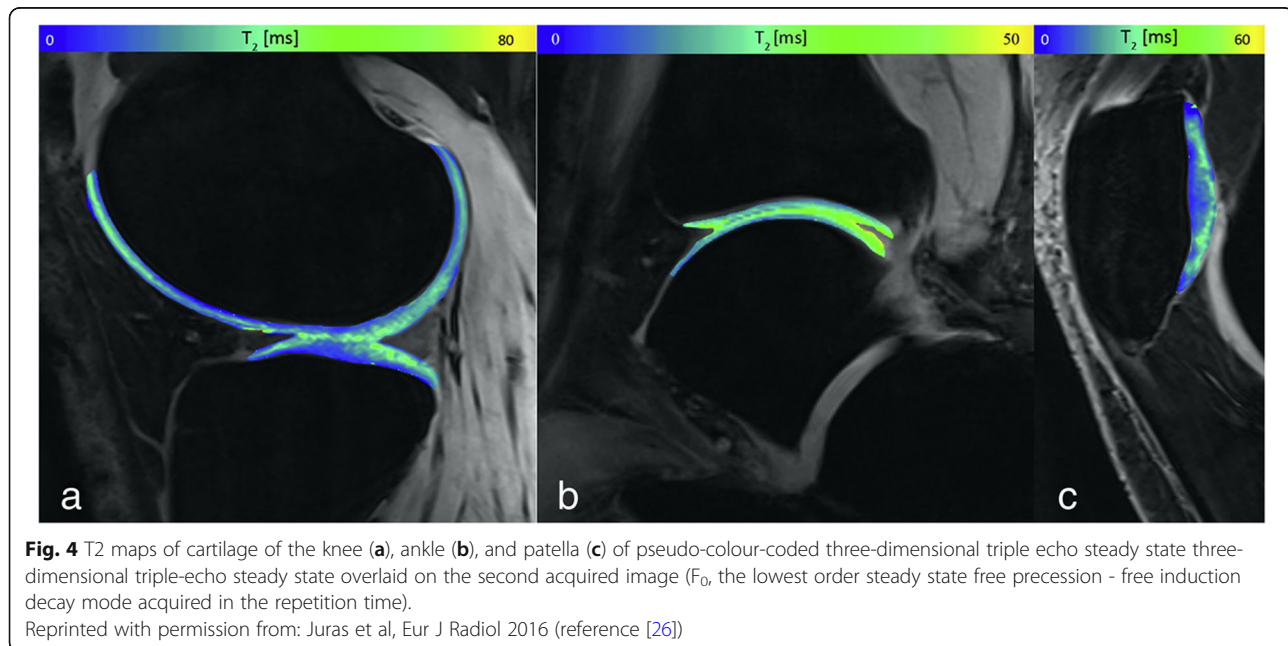
Recently, Juras et al. [19] prospectively evaluated patients with low-grade cartilage lesions at 3 T and and 7 T, demonstrating that 3-T T2 mapping is more sensitive for low-grade lesions than 7-T T2 mapping due to a higher short component of T2, that is considerably reduced at 7 T.

Hip Despite the complex anatomy and the thin layer of cartilage, feasibility of 7-T T2 mapping in the hip was demonstrated by Lazik-Palm et al. [25]. T2 maps with MESE were obtained with minor artefacts, such as pulsation artefacts due to inguinal vessels and inhomogeneities in the dorsal part of the hip. Kraff et al. [22] demonstrated that TESS at 7 T improves quantitative hip cartilage imaging with insensitivity to B₁ inhomogeneities, shortening scan time and comparable quality and repeatability compared to MESE. Feasibility of T2 mapping after cartilage transplant has been demonstrated by Lazik-Palm et al [33], comparing 3-T to 7-T MRI. Despite an apparent overestimation of T2 values at 7 T compared to 3 T, the intra-individual ratio between T2 values of cartilage transplant and normal acetabular and femoral cartilage obtained at 7 T were comparable to that obtained at 3 T, confirming the accuracy of UHF T2 mapping in post-surgical evaluation of the hip [33].

Ankle As for the hip, similar challenges are present for ankle imaging. Domayer et al. [24] demonstrated MESE T2 mapping feasibility, finding a significant zonal differentiation between superficial and deep layer with higher T2 values in the first one. In repair cartilage tissues after surgical treatments, T2 values in the superficial layers were similar to regular cartilage; the deep layers showed significantly increased T2 values, reflecting the abnormal increased water content and lower collagen and glycosaminoglycan (GAG) concentration in reparative tissues. Juras et al. [26] successfully tested 3D TESS T2 mapping in the ankle, finding significant differences of T2 values in the ankle compared to the knee (Fig. 4; see Table 2).

Compositional imaging: T2* mapping

T2* relaxation time reflects the different properties of cartilage extracellular matrix and is obtained with multi-echo GRE T2*-weighted sequences, with at least six echo times. As for T2, T2* shows a zonal differentiation increasing from the deep to the superficial layer, with a



larger gap of T_2^* compared to T_2 . This effect reflects the susceptibility fields induced by the cartilage-to-bone interface with T_2^* shortening [28]. Compared to MESE T_2 mapping, T_2^* mapping allows 3D acquisition and shorter acquisition times, due to a reduced repetition time. However, this technique is more prone to susceptibility artefacts (which are greater at 7 T) that could affect the precision of T_2^* quantification, especially in case of periarticular calcification and subchondral sclerosis. Compared to 3-T MRI, 7-T MRI showed a reduced knee cartilage T_2^* values with a less pronounced zonal differentiation between deep and superficial layer [23].

Compositional imaging: T1rho mapping

Spin-lattice relaxation time in the rotating frame ($T_{1\rho}$) mapping reflects proteoglycan (PG) and collagen cartilage content and has been tested at 7 T in knee and hip joints [25, 32]. In damaged cartilage, characterised by a decreased content of PG, $T_{1\rho}$ values tend to increase due to the altered spine-lattice exchanges between protons and the environment. In particular, even if no changes were observed in T_2 mapping, slight decrease of PG content was observed with $T_{1\rho}$ technique, allowing to detect subtle initial degenerative changes in ageing cartilage [34]. Singh et al. [35] obtained high-SNR and high-resolution 3D $T_{1\rho}$ mapping of the knee cartilage at 7 T with an in-plane resolution of 0.2 mm^2 . Compared to 3 T, at 7 T they reached the same resolution in a four-fold reduced scanning time.

Wyatt et al. [32] compared $T_{1\rho}$ mapping of the knee in healthy volunteers and patients with OA at 3 T and 7 T and found increased $T_{1\rho}$ values in the patellar

cartilage in patient with OA at both field strengths. In the lateral femoral condyle, the same results were obtained at 3 T but were not observed at 7 T. However, many cartilage regions approached significance at UHF and all the p values were lower than those obtained at 3 T, confirming UHF as a promising tool despite the need for further studies to consolidate its superiority.

Compositional imaging: delayed gadolinium-enhanced MRI of cartilage

The first MRI contrast medium introduced in clinical practice is gadopentetate dimeglumine (Gd-DTPA^{2-}). Due to its anion form, it is repelled by the negatively charged GAGs and, thus, it is used to estimate GAGs content in the cartilage. Areas of damaged cartilage, with reduced GAGs content, tend to accumulate Gd-DTPA^{2-} , resulting in shorter T_1 values.

Welsch et al. [28] demonstrated delayed gadolinium-enhanced MRI of cartilage (dGEMRIC) *in vivo* feasibility at 7 T in the knee with T_1 mapping acquisitions in healthy volunteers before and 90 min after intravenous Gd-DTPA^{2-} administration, asking the subjects to exercise the knee for 20 min. Although T_1 values at 7 T were lower compared to those obtained at lower field strengths, the use of pre-/post-contrast ratio represents a promising tool to estimate GAGs content in native and repair cartilage.

Potential future introduction of this technique in clinical practice will benefit from a reduction in scanning time, which can be obtained omitting the pre-contrast T_1 mapping acquisition. Indeed, post-contrast T_1 values were demonstrated sufficient to assess the cartilage health status in the hip at 7 T thanks to its linear

correlation with the difference in relaxation rate between pre-contrast and post-contrast T1 values [25].

Despite the high specificity for GAGs, long scanning time, need for post-injection exercise and intravenous contrast medium administration limit the dGEMRIC technique, which result in being more invasive and expensive than others. Moreover, evidences for gadolinium retention in the brain (and in other human tissues) have been published, although no clinically or biologically relevant consequences have been demonstrated, yet [36].

Compositional imaging: diffusion tensor imaging

Since different components of the cartilage matrix affect the motion of water molecules, diffusion tensor imaging can provide information about PG content and collagen architecture. PGs lead to a motion restriction in all the directions, affecting the mean diffusivity. Collagen network induces anisotropy in the water motion, which can be measured with fractional anisotropy [37]. Although diffusion techniques are challenging at UHF, Raya et al. [38] succeeded in patellar cartilage evaluation at 7 T using line-scan DT imaging. It is inherently insensitive to motion artefacts and B_1 , B_0 and susceptibility inhomogeneity; the poor SNR was overcome by using UHF MRI and multi-channel coils. Matrix alterations led to increased apparent diffusion coefficient (ADC) and reduced fractional anisotropy, permitting to significantly differentiate damaged from healthy cartilage. Damaged cartilage showed increased ADC values both in the superficial and in the deep layers, showing a promising role of ADC as early indicator of cartilage degeneration.

Compositional imaging: magnetisation transfer

In cartilage, there are two proton pools in biochemical and magnetic equilibrium: free (unbound) water protons, visible by MRI, and macromolecules-bound protons, not visible by MRI. When bound protons are saturated by off-resonance pulses, the equilibrium shifts in favour of bound protons, reducing the detectable magnetisation and the signal. Therefore, magnetisation transfer acquisition, based on steady state free precession sequences, can provide quantitative biochemical cartilage evaluation [30]. At 7 T, knee cartilage magnetisation transfer showed significantly reduced mean values compared to 3 T with a significant zonal stratification detectable only at 7 T [23].

Compositional imaging: chemical exchange saturation transfer

GagCEST method estimates the cartilage GAG content by selective saturation of protons within the hydroxyl groups of cartilage GAGs, reducing the signal intensity due to the magnetisation exchange with free water. UHF MRI improves the gagCEST performance for the increased SNR as well as for the more selective saturation

between hydroxyl GAG and water protons due to the increased gap in resonance frequencies [18, 38–40].

The first gagCEST application at 7 T was performed for post-surgical knee cartilage evaluation [41]. GagCEST feasibility and its role as a potential imaging biomarker of cartilage GAG content was proven, based on its correlation with the high-GAG-specific sodium imaging [41]. A 3 T *versus* 7 T comparison study stated the need for UHF MRI to accurately estimate GAGs avoiding direct saturation effects and fast exchange rate observed at 3 T [42]. Regarding post-surgical long-term cartilage evaluation, a significant GAGs reduction in repair cartilage compared to native cartilage was demonstrated, albeit without significant correlation with the clinical outcome [31].

Promising results have been obtained by applying modified technical parameters to selectively optimise the chemical exchange saturation transfer (CEST) signal from hydroxyl protons of exogenous hyaluronic acids (HAs) to evaluate their distribution in the cartilage (viscoCEST). Compared to viscoCEST, gagCEST detected signal also from exogenous GAGs, while viscoCEST was not able to depict endogenous GAGs. This could represent a promising tool to track the intraarticular distribution of hyaluronic acid after viscosupplementation [43].

Compositional imaging: sodium

The negatively charged lateral chains of GAG within the cartilage attract sodium atoms, making sodium signal an imaging biomarker for the cartilage matrix. UHF MRI performed with dedicated coils permits to partially overcome the 3,000 times lower SNR of sodium compared to proton [18].

Wang et al. [44] first obtained 3D sodium images of the whole knee at 7 T in less than 15 min with a 3D GRE sequence with radial k-space acquisition. They observed a significant reduction in sodium concentration in patients with OA compared to healthy subjects. Recently, a two-fold reduced scan time was obtained for 7-T MRI of the knee by introducing compressed sensing techniques without losing accuracy in total sodium concentration for detecting early signs of OA [45].

The low sensitivity of sodium imaging requires dedicated and optimised coils; dual tuned coils ($^1\text{H}/^{23}\text{Na}$) have been tested to reduce the reciprocal induced degradation of the sensitivity. Although many progresses have been made, we do not have the optimal coil yet and further efforts are still needed [46, 47]. Moreover, quantitative sodium imaging is affected by partial volume effects including articular fluid. Different inversion recovery techniques have been proved to overcome this challenge, albeit the increase in SAR [48, 49]. For its role in early damaged cartilage evaluation, sodium imaging has been tested for the evaluation of different post-surgical cartilage repair tissues. A significantly lower sodium signal in repair

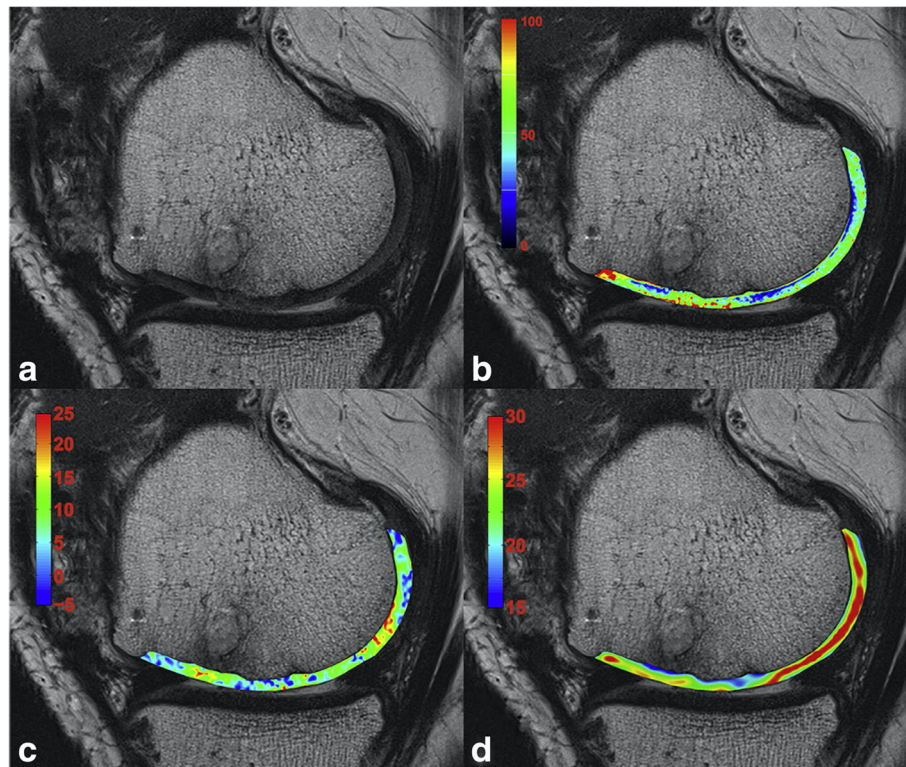


Fig. 5 7-T MRI of a patient (mean age of subjects included: 49 years old; interquartile range, 44–55) 8 years after osteochondral treatment at the medial femoral condyle. **a** Morphologic proton-density fast spin-echo image. **b** Graphical overlay with T2 map. Colour bar represents relaxation times (ms) (higher values, more water and disturbed collagen architecture). **c** Graphical overlay with glycosaminoglycan chemical exchange saturation transfer (gagCEST) image. Colour bar represents gagCEST asymmetries in % (lower values, less proteoglycan content). **d** Graphical overlay with sodium image. Colour bar represents the sodium signal-to-noise ratio values (lower values, less proteoglycan content). Reprinted with permission from: Krusche-Mandl et al., *Osteoarthr Cartil* 2012 (reference [31])

cartilage tissue compared to native cartilage was observed (Fig. 5). Despite a difference in GAG content in cartilage repair tissues after surgical treatments, no significant difference for the clinical outcomes among the different surgical approaches was demonstrated [31, 50].

Bone

Many studies have been performed focusing on trabecular bone quantitative evaluation in osteoporosis and OA. Mechanical properties of the trabecular bone depend not only on the bone volume fraction (density) but also on the internal arrangement. While usual clinical techniques, such as dual-energy x-ray absorptiometry, evaluate bone density alone, novel methods called micro-finite element (micro-FE) techniques estimate every aspect of bone internal architecture through reconstruction and modelling of high-resolution 3D datasets. So far, these datasets could be given by micro-computed tomography, limiting this approach to small size bone/bone samples [51]. Chang et al. [52] demonstrated the feasibility of micro-FE of the knee providing high-resolution 3D datasets with 3D fast low angle shot acquisitions at 7 T. With a 7-min scan, they could

differentiate contributions of trabecular and cortical bone to the whole bone stiffness. Trabecular bone resulted predominant in long bones epiphyseal stiffness thus representing a better target for treatments in reducing fractures. Combining UHF MRI and micro-FE could help to evaluate bone mechanical competence in osteoporosis and, focusing on subchondral bone, its role in OA pathogenesis.

Regarding 7-T quantitative bone imaging applications, Chang et al. [53] demonstrated an improvement in trabecular bone architecture in response to elevated mechanical stress in athletes.

Krug et al. [54] compared balanced steady state free precession and balanced steady state spin-echo techniques for trabecular bone estimation at 3 T and 7 T. The number of measured trabeculae was more accurate at UHF, albeit some overestimation of trabecular volume occurred due to the increased susceptibility effects. A bigger potential for UHF balanced steady state spin-echo technique was suggested due to the reduced off-resonance artefacts which cause trabecular broadening and small trabeculae disappearance.

Preliminary data of 7-T *ex vivo* studies demonstrated feasibility of ultrashort time of echo (UTE) T2* mapping

of cortical bone with high-resolution isotropic acquisition [55] and suggested potential applications in the spine [56]. Finally, Li et al. [57] demonstrated feasibility of 7-T MRI of bone marrow perfusion of the distal femur without intravenous administration of contrast agent using the arterial spin labelling approach, although further technical developments are needed.

Ligaments and tendons

Conventional MRI visualisation of tendons and ligaments can be difficult due to the low signal given by their short T2 [58]. Among the novel sequences, UTE has been demonstrated useful to better depict these structures [59], including the fascicular pattern in the Achilles tendon with stripes of higher signal representing endotendon and inner areas of lower signal representing fascicles. Similarly, in the knee, different structures like tendons, ligaments and menisci were depicted in less than 5 min with 0.7–0.8-mm isotropic resolution [60].

Juras et al. [61] compared 3-T and 7-T 3D UTE T2* mapping of the Achilles tendon in volunteers and in patients with tendinopathy. Interestingly, SNR was higher at 3 T while the contrast was almost double at 7 T. A significant increase in T2* values in patients compared to healthy volunteers was observed. Since T2* mapping resulted sensitive for biochemical changes related to tendinopathy, it could represent a useful imaging biomarker for early detection of tendon degeneration. The same technique with fat saturation led to a better microstructure visualisation of the Achilles tendon with improved SNR at 7 T compared to 3 T [62]. Regarding sodium imaging, Juras et al. [63] demonstrated a significant increase in sodium signal in patients with tendinopathy compared to healthy volunteers (Fig. 6), reflecting the increase in GAG content. The authors found an increased amount of GAGs not only in the area of

tendinopathy depicted by morphological imaging but also in the whole tendon, with a possible role in detecting patients at risk for Achilles tendon tear [63].

A comparison between 7-T MRI and arthroscopy of the shoulder has been performed by Lazik-Palm et al. [17], demonstrating the feasibility of clinical protocol acquisition at 7 T with diagnostic image quality in patients with suspected tendinopathy of the rotator cuff. Compared to the arthroscopic evaluation, 7-T MRI led to an overestimation of tendinopathy, especially regarding supraspinatus and subscapularis tendons. This was explained by the authors, on the one hand, with the interpretation bias due to the magic angle effect, which creates artefactual hyperintensities in structures orientated at 55° to the main magnetic field, even if reduced compared to lower field strengths. On the other hand, the expected higher resolution of 7-T imaging and the patient selection criteria might have led to a misinterpretation of the signal alterations [17]. At the state of the art, the diagnostic accuracy of 3-T MRI still remains superior to 7-T MRI of the shoulder [17] and further studies are needed in order to include UHF-MRI of the shoulder in clinical practice.

Concerning ligaments, Anz et al. [64] compared 7-T and 3-T quantitative evaluation of T2/T2* values and volumes of the anterior cruciate ligament in the knee of 30 healthy volunteers (Table 3). An accurate quantitative evaluation of the anterior cruciate ligament might represent a promising tool to assess the “*ligamentisation*” process of tendon grafts after surgery. Despite these results, no demonstrable advantage in 7-T MRI over 3-T MRI was observed.

Menisci and intervertebral discs

As for other connective tissues, meniscal MRI visualisation benefits from UHF: higher SNR, higher resolution and better contrast at 7 T enable a more accurate detection of

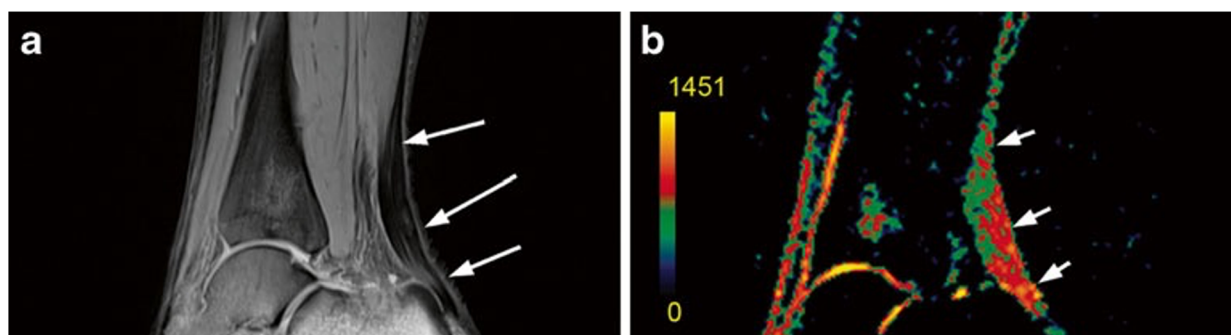


Fig. 6 MRI of a 46-year-old patient with chronic Achilles tendinopathy. **a** Proton-density-weighted two-dimensional turbo spin-echo image depicts centres of each region of interest (arrows). **b** Corresponding colour-coded three-dimensional gradient-echo sodium image depicts Achilles tendon sodium signal (arrows), which is obviously higher than that in the healthy volunteer. The sodium signal increase was observed in the whole tendon, and not only in regions with clinical findings (middle region in this case). All patients had focal thickening of the Achilles tendon without fluid-like signal intensity increase on proton-density-weighted two-dimensional turbo spin-echo images. Colour scale represents sodium signal intensity values.

Reprinted with permission from: Juras et al., *Radiology* 2012 (reference [63])

Table 3 Anterior cruciate ligament quantitative MRI at 3 T and 7 T

Field strength	T2 values (ms) Mean ± SD	T2* values (ms) Mean ± SD	Volume (mm ³) Mean ± SD
3 T	37.1 ± 7.9	10.9 ± 1.3	2,380 ± 602
7 T	39.7 ± 6.2	10.9 ± 0.9	2,484 ± 736

Source: Anz et al., *Skeletal Radiol* 2020—reference [64]. SD Standard deviation

subtle morphological meniscal alterations compared to clinical field strengths [7]. UHF MRI also allows T2* quantification of the meniscal ultrastructure with a demonstrated relationship between T2* decay and collagen fibres orientation. Although further studies are needed to transfer this method into the clinical practice, these results might help in the interpretation of T2 and T2* quantitative images of early meniscal degeneration at clinical field strengths with lower resolution [65]. Important information on disc ultrastructure and degeneration was obtained *ex vivo* with a correlation between matrix degeneration and distribution of PG diffusivity and PG CEST. Thus, ADC and CEST values have been proposed as imaging biomarkers of early disc degeneration. Moreover, PG T2 values correlated only with severe disc degeneration [66].

Feasibility of disc sodium imaging and T2 mapping *in vivo* at 7 T was first demonstrated by Noebauer-Huhmann et al. [67], who performed a comparison with a semiquantitative morphological score for intervertebral disc degeneration (Pfirrmann score [68]) in healthy volunteers. Sodium imaging and T2 maps values showed a positive correlation and a moderate negative correlation with the Pfirrmann score respectively, while no correlation was found between sodium and T2 values. This work paved the way for future *in vivo* applications in the disc degeneration assessment.

Muscles

Muscles can be evaluated by MRI in terms of structural and functional imaging. Despite the improved SNR and the higher resolution, no morphological UHF studies have been performed in muscles, yet. Integrating 7-T images with data from computed tomography, Kerkhof et al. [69] created an *ex vivo* complete 3D highly accurate virtual musculoskeletal model of forearm and hand, including relevant physiological parameters. This open-source study provides a free 3D anatomical model useful for further studies in physio-pathological musculoskeletal research.

Many studies confirmed UHF advantages for magnetic resonance spectroscopy (MRS) due to the improved spectral resolution and the capability of X-nuclei imaging [70]. Among the different nuclei, phosphorus (³¹P) is the main target of UHF evaluation of muscles. In particular, many papers focused on inorganic phosphorus and phosphorylated metabolites estimation to assess mitochondrial function in skeletal muscles recovery. Kan et al. [71] first published data obtained with direct *in vivo* quantification

of the inorganic phosphate pool (P_i) in resting muscles in healthy subjects at 7 T. The transmit and receive dual-tuned (¹H/³¹P) coil, the high SNR, the improved spectral and spatial resolution permitted to differentiate cytosolic P_i from mitochondrial P_i. At the same time, signals from phosphorylated muscle metabolites, usually observable at lower field strengths, were also detectable at 7 T.

Subsequent works confirmed the gain in spectral, temporal and spatial resolution obtained at 7 T for ³¹P imaging to investigate muscle recovery with different techniques at rest and during exercise [72, 73]. Multiple phosphate metabolites as well as the single metabolite estimation can be performed with different techniques, with consequent influence on the total scan time [72].

Recently, quantitative detailed dynamic evaluation of muscles metabolism has been demonstrated to be feasible thanks to the higher SNR provided by dedicated coils, efficient localisation and UHF. Additionally, cytosolic buffer capacity and H⁺ efflux from muscle cells to blood in early recovery were non-invasively quantified for the first time [73].

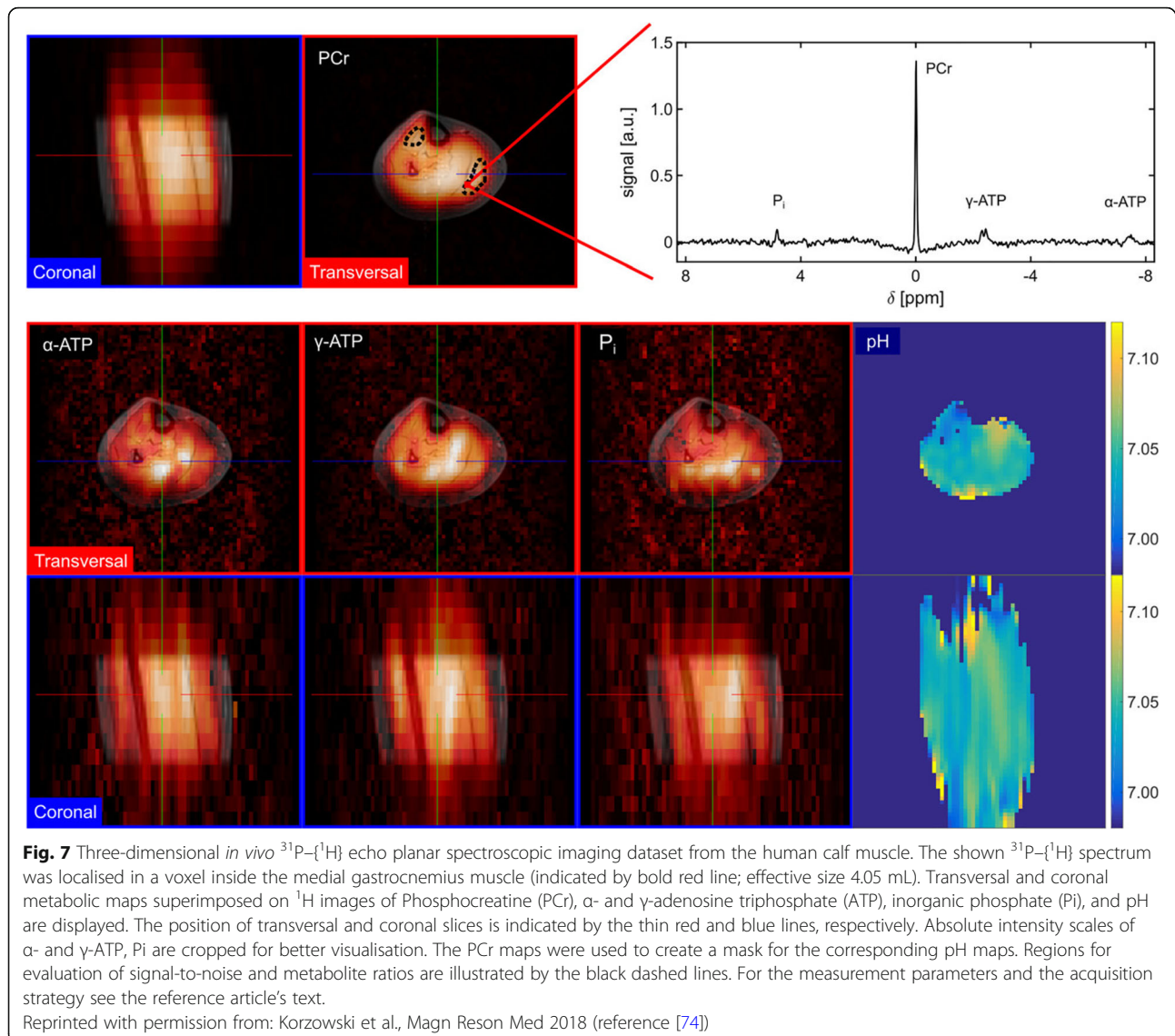
Last updates on ³¹P imaging demonstrated feasibility of high-resolution ³¹P imaging performed with multishot 3D echo planar spectroscopic imaging instead of the more used chemical shift imaging. This novel approach permitted to obtain high-resolution 3D mapping of ³¹P-metabolites and intracellular pH reducing the scan time up to 10 min with a voxel size of 4 cm³ (Fig. 7) [74].

To indirectly estimate creatine (Cr) concentration, CrCEST technique exploits the chemical exchange saturation transfer effect between its amine and bulk water protons. In addition to the good agreement between CrCEST and ³¹P MRS in the recovery kinetics after exercise, CrCEST provides a three-fold sensitivity enhancement compared to ³¹P MRS [75]. Recently, Kogan et al. [76] demonstrated that CrCEST in the lower leg muscles of healthy volunteers at 7 T is not influenced by blood flow during recovery.

Several promising techniques to non-invasively investigate the different characteristics of skeletal muscles were tested at UHF, including potassium MRS for intracellular evaluation [77] and ¹³Carbon MRS for absolute quantitative assessment of intramuscular glycogen in storage diseases [78]. Finally, Towse et al. [79] compared the blood oxygenation-level dependence technique in healthy volunteers, demonstrating a significant increase in CNR and SNR in the evaluation of muscles microcirculation at 7 T compared to 3 T.

Limitations

While specific limitations of each technique are discussed above, general limitations that could affect image quality at UHF are B₁ and B₀ inhomogeneities, increased T1 relaxation times and decreased T2 relaxation times, which require mandatory time-consuming preliminary optimisation. Increased susceptibility and chemical shift, exploited for specific diagnostic purposes, also lead to



artefacts. At UHF, higher RFs and shorter wavelengths may result in decreased penetration with inhomogeneous excitation. Indeed, these also cause increased SAR [38]. MRI below 8 T is considered safe by FDA; nevertheless, SAR limits are established [80]. While global SAR limits are usually respected in MSK UHF MRI, attention must be paid to potential local SAR increase.

Different prediction methods for SAR spatial distribution, including machine learning, have been tested to prevent potential health risks for patients [81, 82].

Although an increase in physiologic side effects have been reported at UHF (dizziness, nausea and metallic taste) [83, 84], patients' experience seems to be similar to that perceived at lower field strengths [85].

Finally, the high costs for installation and maintenance of UHF MRI scanners and their low availability actually

represent a not negligible limitation for their routine clinical use.

Future perspectives and conclusions

Future perspectives will depend on the constantly evolving innovation in hardware/software and sequences, such as implementation of parallel imaging [6, 86], B_1 shimming techniques [87] and MRI fingerprinting [88]. Another fascinating novel application is represented by early detection of synovitis in rheumatoid arthritis, even though still tested in animal models [89]. As in other fields [90, 91], staging of bone tumours in children could be a future potential application of UHF MRI, exploiting the high spatial resolution to better define the growth plate invasion with potentially less invasive surgical treatments and improved quality of life. The higher SNR could also provide a more

accurate visualisation of vessels both with and without intravenous administration of contrast agent [92].

In conclusion, UHF MRI provides important diagnostic improvements in the field of MSK imaging. Higher SNR and CNR permits to obtain higher spatiotemporal resolution with improved anatomic detail of the musculoskeletal structures and higher diagnostic confidence. Additionally, improvements in spectroscopic and quantitative imaging provide biochemical and metabolic information allowing a better tissue characterisation. Approvals for clinical imaging at UHF were the first step towards a routine use of this technology. However, studies are needed to consolidate the advantages of a routine clinical utilisation of UHF-MRI. To overcome its limitations, promising efforts in hardware and software development are already in progress.

Abbreviations

ADC: Apparent diffusion coefficient; CEST: Chemical exchange saturation transfer; CNR: Contrast-to-noise ratio; Cr: Creatine; FDA: Food and Drugs Administration; GAGs: Glycosaminoglycans; Gd-DTPA: Gadopentetate dimeglumine; GRE: Gradient echo; MESE: Multi-echo spin-echo; Micro-FE: Micro-finite element; MRI: Magnetic resonance imaging; MRS: Magnetic resonance spectroscopy; MSK: Musculoskeletal; OA: Osteoarthritis; PG: Proteoglycan; Pi: Inorganic phosphate pool; RF: Radiofrequency; SAR: Specific absorption rate; SNR: Signal-to-noise ratio; T1rho: Spin-lattice relaxation time in the rotating frame; TESS: Triple echo steady state; TSE: Turbo spin-echo; UHF: Ultra-high field; UTE: Ultrashort time of echo

Acknowledgements

We would like to acknowledge the team of the Imago7 Foundation (Pisa, Italy) for the collaboration.

Authors' contributions

All authors were involved in drafting the article or revising it critically for the intellectual content. AG performed literature research, table creation and figure selection. ZV and TM provided a fundamental contribution respectively to clinical and physical text revision.

Funding information

This research received no specific grant from any funding agency in the public, commercial, or not-for-profit sectors.

Availability of data and materials

Not applicable.

Ethics approval and consent to participate

Not applicable.

Consent for publication

Not applicable.

Competing interests

The authors have nothing to disclose.

Author details

¹Department of Translational Research and New Technologies in Medicine and Surgery, University of Pisa, Via Risorgimento, 36 Pisa, Italy. ²Diagnostic and Interventional Radiology, University Hospital of Pisa, Via paradisa, 2, Pisa, Italy. ³Imago 7 Foundation, Viale del Tirreno, 331 Pisa, Italy.

Received: 20 March 2020 Accepted: 1 July 2020

Published online: 06 August 2020

References

- Gruetter R, Henry P-G, Hongxia L et al (2006) In-vivo NMR spectroscopy of the brain at high fields. In: Robitaille P-M, Berliner L (eds) Ultra high field magnetic resonance imaging. Springer, Boston, MA, pp 373–410
- Medgadget.com (2017) EU gives first approval for ultra-high-field MRI scanner, The Siemens Magnetom Terra. <https://www.medgadget.com/2017/08/eu-gives-first-approval-ultra-high-field-mri-scanner-siemens-magnetom-terra.html>
- Medgadget.com (2017) FDA gives first clearance to Siemens high-field 7 Tesla MRI scanner. <https://www.medgadget.com/2017/10/fda-gives-first-clearance-high-field-7-tesla-mri-scanner.html>
- Banerjee S, Krug R, Carballido-Gamio J et al (2008) Rapid in vivo musculoskeletal MR with parallel imaging at 7T. *Magn Reson Med* 59:655–660 <https://doi.org/10.1002/mrm.21455>
- Mugler JP 3rd (2014) Optimized three-dimensional fast-spin-echo MRI. *J Magn Reson Imaging* 39:745–767 <https://doi.org/10.1002/jmri.24542>
- Jin J, Weber E, Destruel A et al (2018) An open 8-channel parallel transmission coil for static and dynamic 7T MRI of the knee and ankle joints at multiple postures. *Magn Reson Med* 79:1804–1816 <https://doi.org/10.1002/mrm.26804>
- Regatte RR, Schweitzer ME (2007) Ultra-high-field MRI of the musculoskeletal system at 7.0T. *J Magn Reson Imaging* 25:262–269 <https://doi.org/10.1002/jmri.20814>
- Stahl R, Krug R, Kelley DAC et al (2009) Assessment of cartilage-dedicated sequences at ultra-high-field MRI: comparison of imaging performance and diagnostic confidence between 3.0 and 7.0 T with respect to osteoarthritis-induced changes at the knee joint. *Skeletal Radiol* 38:771–783 <https://doi.org/10.1007/s00256-009-0676-z>
- Behr B, Stadler J, Michaely HJ, Damert HG, Schneider W (2009) MR imaging of the human hand and wrist at 7 T. *Skeletal Radiol* 38:911–917 <https://doi.org/10.1007/s00256-009-0673-2>
- Theysohn JM, Kraff O, Orzada S et al (2013) Bilateral hip imaging at 7 Tesla using a multi-channel transmit technology: initial results presenting anatomical detail in healthy volunteers and pathological changes in patients with avascular necrosis of the femoral head. *Skeletal Radiol* 42:1555–1563 <https://doi.org/10.1007/s00256-013-1698-0>
- Springer E, Bohndorf K, Juras V et al (2017) Comparison of routine knee magnetic resonance imaging at 3 T and 7 T. *Invest Radiol* 52:42–54 <https://doi.org/10.1097/RLI.0000000000000303>
- Welsch GH, Juras V, Szomolanyi P et al (2012) Magnetic resonance imaging of the knee at 3 and 7 Tesla: a comparison using dedicated multi-channel coils and optimised 2D and 3D protocols. *Eur Radiol* 22:1852–1859 <https://doi.org/10.1007/s00330-012-2450-1>
- Aringhieri G, Vitali S, Rossi P, Caramella D (2018) The new frontier of imaging: the micron. *Clin Exp Rheumatol* 36
- He X, Ertürk MA, Grant A et al (2019) First in-vivo human imaging at 10.5T: imaging the body at 447 MHz. *Magn Reson Med* 84:289–303 <https://doi.org/10.1002/mrm.28131>
- Juras V, Welsch G, Bär P, Kronnerwetter C, Fujita H, Trattng S (2012) Comparison of 3 T and 7 T MRI clinical sequences for ankle imaging. *Eur J Radiol* 81:1846–1850 <https://doi.org/10.1016/j.ejrad.2011.05.023>
- Theysohn JM, Kraff O, Maderwald S et al (2013) MRI of the ankle joint in healthy non-athletes and in marathon runners: image quality issues at 7.0 T compared to 1.5 T. *Skeletal Radiol* 42:261–267 <https://doi.org/10.1007/s00256-012-1454-x>
- Lazik-Palm A, Kraff O, Rietsch SHG et al (2020) 7-T clinical MRI of the shoulder in patients with suspected lesions of the rotator cuff. *Eur Radiol Exp* 4:1–9 <https://doi.org/10.1186/s41747-019-0142-1>
- Juras V, Mlynarik V, Szomolanyi P, Valkovič L, Trattng S (2019) Magnetic resonance imaging of the musculoskeletal system at 7T: morphological imaging and beyond. *Top Magn Reson Imaging* 28:125–135 <https://doi.org/10.1097/RMR.0000000000000205>
- Juras V, Schreiner M, Laurent D et al (2019) The comparison of the performance of 3 T and 7 T T2 mapping for untreated low-grade cartilage lesions. *Magn Reson Imaging* 55:86–92 <https://doi.org/10.1016/j.mri.2018.09.021>
- Heule R, Ganter C, Bieri O (2014) Triple echo steady-state (TESS) relaxometry. *Magn Reson Med* 71:230–237 <https://doi.org/10.1002/mrm.24659>

21. Juras V, Bohndorf K, Heule R et al (2016) A comparison of multi-echo spin-echo and triple-echo steady-state T2 mapping for in vivo evaluation of articular cartilage. *Eur Radiol* 26:1905–1912 <https://doi.org/10.1007/s00330-015-3979-6>
22. Kraff O, Lazik-Palm A, Heule R, Theysohn JM, Bieri O, Quick HH (2016) 7 Tesla quantitative hip MRI: a comparison between TESS and CPMG for T2 mapping. *MAGMA* 29:503–512 <https://doi.org/10.1007/s10334-016-0557-0>
23. Welsch GH, Apprich S, Zbyn S et al (2011) Biochemical (T2, T2* and magnetisation transfer ratio) MRI of knee cartilage: Feasibility at ultra-high field (7T) compared with high field (3T) strength. *Eur Radiol* 21:1136–1143 <https://doi.org/10.1007/s00330-010-2029-7>
24. Domayer SE, Apprich S, Stelzener D et al (2012) Cartilage repair of the ankle: first results of T2 mapping at 7.0 T after microfracture and matrix associated autologous cartilage transplantation. *Osteoarthritis Cartilage* 20: 829–836 <https://doi.org/10.1016/j.joca.2012.04.015>
25. Lazik A, Theysohn JM, Geis C et al (2016) 7 Tesla quantitative hip MRI: T1, T2 and T2* mapping of hip cartilage in healthy volunteers. *Eur Radiol* 26:1245–1253 <https://doi.org/10.1007/s00330-015-3964-0>
26. Juras V, Zbyň Š, Mlynarik V et al (2016) The compositional difference between ankle and knee cartilage demonstrated by T2 mapping at 7 Tesla MR. *Eur J Radiol* 85:771–777 <https://doi.org/10.1016/j.ejrad.2016.01.021>
27. Lazik-Palm A, Kraff O, Geis C et al (2016) Morphological imaging and T2 and T2* mapping of hip cartilage at 7 Tesla MRI under the influence of intravenous gadolinium. *Eur Radiol* 26:3923–3931 <https://doi.org/10.1007/s00330-016-4247-0>
28. Welsch GH, Mamish TC, Hughes T et al (2008) In vivo biochemical 7.0 Tesla magnetic resonance: preliminary results of dGEMRIC, zonal T2, and T2* mapping of articular cartilage. *Invest Radiol* 43:619–626 <https://doi.org/10.1097/rli.0b013e31817e9122>
29. Smith HE, Mosher TJ, Dardzinski BJ et al (2001) Spatial variation in cartilage T2 of the knee. *J Magn Reson Imaging* 14:50–55 <https://doi.org/10.1002/jmri.1150>
30. Welsch GH, Trattig S, Scheffler K et al (2008) Magnetization transfer contrast and T2 mapping in the evaluation of cartilage repair tissue with 3T MRI. *J Magn Reson Imaging* 28:979–986 <https://doi.org/10.1002/jmri.21516>
31. Krusche-Mandl I, Schmitt B, Zak L et al (2012) Long-term results 8 years after autologous osteochondral transplantation: 7 T gagCEST and sodium magnetic resonance imaging with morphological and clinical correlation. *Osteoarthritis Cartilage* 20:357–363 <https://doi.org/10.1016/j.joca.2012.01.020>
32. Wyatt C, Guha A, Venkatachari A et al (2015) Improved differentiation between knees with cartilage lesions and controls using 7T relaxation time mapping. *J Orthop Transl* 3:197–204 <https://doi.org/10.1016/j.jot.2015.05.003>
33. Lazik-Palm A, Kraff O, Johst S et al (2016) Morphological and quantitative 7 T MRI of hip cartilage transplants in comparison to 3 T-initial experiences. *Invest Radiol* 51:552–559 <https://doi.org/10.1097/RLI.0000000000000264>
34. Li X, Benjamin Ma C, Link TM et al (2007) In vivo T1 ρ and T2 mapping of articular cartilage in osteoarthritis of the knee using 3 T MRI. *Osteoarthritis Cartilage*. <https://doi.org/10.1016/j.joca.2007.01.011>
35. Singh A, Haris M, Cai K, Kogan F, Hariharan H, Reddy R (2014) High resolution T1 ρ mapping of in vivo human knee cartilage at 7T. *PLoS One* 9: 3–11 <https://doi.org/10.1371/journal.pone.0097486>
36. Gulani V, Calamante F, Shellock FG, Kanal E, Reeder SB; International Society for Magnetic Resonance in Medicine (2017) Gadolinium deposition in the brain: summary of evidence and recommendations. *Lancet Neurol* 16:564–570 [https://doi.org/10.1016/S1474-4422\(17\)30158-8](https://doi.org/10.1016/S1474-4422(17)30158-8)
37. Raya JG (2015) Techniques and applications of in vivo diffusion imaging of articular cartilage. *J Magn Reson Imaging* 41:1487–1504 <https://doi.org/10.1002/jmri.24767>
38. Alizai H, Chang G, Regatte RR (2018) MR imaging of the musculoskeletal system using ultrahigh field (7T) MR imaging. *PET Clin* 13:551–565 <https://doi.org/10.1016/j.cpet.2018.05.008>
39. Oei EHG, Van Tiel J, Robinson WH, Gold GE (2014) Quantitative radiologic imaging techniques for articular cartilage composition: toward early diagnosis and development of disease-modifying therapeutics for osteoarthritis. *Arthritis Care Res (Hoboken)* 66:1129–1141 <https://doi.org/10.1002/acr.22316>
40. Trattig S, Zbyň Š, Schmitt B et al (2012) Advanced MR methods at ultra-high field (7 Tesla) for clinical musculoskeletal applications. *Eur Radiol* 22: 2338–2346 <https://doi.org/10.1007/s00330-012-2508-0>
41. Schmitt B, Zbyň Š, Stelzener D et al (2011) Cartilage quality assessment by using glycosaminoglycan chemical exchange saturation transfer and 23Na MR imaging at 7 T. *Radiology* 260:257–264 <https://doi.org/10.1148/radiol.11101841/-/DC1>
42. Singh A, Haris M, Cai K et al (2012) Chemical exchange saturation transfer magnetic resonance imaging of human knee cartilage at 3 T and 7 T. *Magn Reson Med* 68:588–594 <https://doi.org/10.1002/mrm.23250>
43. Haris M, Singh A, Reddy S et al (2016) Characterization of viscosupplementation formulations using chemical exchange saturation transfer (ViscoCEST). *J Transl Med* 14:1–6 <https://doi.org/10.1186/s12967-016-0850-8>
44. Wang L, Wu Y, Chang G et al (2009) Rapid isotropic 3D-sodium MRI of the knee joint in vivo at 7T. *J Magn Reson Imaging* 30:606–614 <https://doi.org/10.1002/jmri.21881>
45. Madelin G, Chang G, Otazo R, Jerschow A, Regatte RR (2012) Compressed sensing sodium MRI of cartilage at 7T: Preliminary study. *J Magn Reson* 214: 360–365 <https://doi.org/10.1016/j.jmr.2011.12.005>
46. Wiggins GC, Brown R, Lakshmanan K (2016) High-performance radiofrequency coils for 23Na MRI: Brain and musculoskeletal applications. *NMR Biomed* 29:96–106 <https://doi.org/10.1002/nbm.3379>
47. Moon CH, Kim JH, Zhao T, Bae KT (2013) Quantitative 23Na MRI of human knee cartilage using dual-tuned 1H/23Na transmitter array radiofrequency coil at 7 tesla. *J Magn Reson Imaging* 38:1063–1072 <https://doi.org/10.1002/jmri.24030>
48. Madelin G, Lee JS, Inati S, Jerschow A, Regatte RR (2010) Sodium inversion recovery MRI of the knee joint in vivo at 7T. *J Magn Reson* 207:42–52 <https://doi.org/10.1016/j.jmr.2010.08.003>
49. Xia D, Lee JS, Regatte RR (2018) Quadrupolar jump-and-return pulse sequence for fluid-suppressed sodium MRI of the knee joint at 7T. *Magn Reson Med* 80:641–647 <https://doi.org/10.1002/mrm.27047>
50. Zbyň Š, Stelzener D, Welsch GH et al (2012) Evaluation of native hyaline cartilage and repair tissue after two cartilage repair surgery techniques with 23Na MR imaging at 7 T: Initial experience. *Osteoarthritis Cartilage* 20:837–845 <https://doi.org/10.1016/j.joca.2012.04.020>
51. Van Rietbergen B, Majumdar S, Pistoia W et al (1998) Assessment of cancellous bone mechanical properties from micro-FE models based on micro-CT, pQCT and MR images. *Technol Health Care* 6:413–420 <https://doi.org/10.3233/thc-1998-65-613>
52. Chang G, Rajapakse CS, Babb JS, Honig SP, Recht MP, Regatte RR (2012) In vivo estimation of bone stiffness at the distal femur and proximal tibia using ultra-high-field 7-Tesla magnetic resonance imaging and micro-finite element analysis. *J Bone Miner Metab* 30:243–251 <https://doi.org/10.1007/s00774-011-0333-1>
53. Chang G, Pakin SK, Schweitzer ME, Saha PK, Regatte RR (2008) Adaptations in trabecular bone microarchitecture in olympic athletes determined by 7T MRI. *J Magn Reson Imaging* 27:1089–1095 <https://doi.org/10.1002/jmri.21326>
54. Krug R, Carballido-Gamio J, Banerjee S, Burghardt AJ, Link TM, Majumdar S (2008) In vivo ultra-high-field magnetic resonance imaging of trabecular bone microarchitecture at 7 T. *J Magn Reson Imaging* 27:854–859 <https://doi.org/10.1002/jmri.21325>
55. Krug R, Larson PEZ, Wang C et al (2011) Ultrashort echo time MRI of cortical bone at 7 Tesla field strength: a feasibility study. *J Magn Reson Imaging* 34: 691–695 <https://doi.org/10.1002/jmri.22648>
56. Guenoun D, Fouré A, Pithioux M et al (2017) Correlative analysis of vertebral trabecular bone microarchitecture and mechanical properties: a combined ultra-high field (7 Tesla) MRI and biomechanical investigation. *Spine (Phila Pa 1976)* 42:E1165–E1172 <https://doi.org/10.1097/BRS.00000000000002163>
57. Li X, Johnson CP, Ellermann J (2019) 7T bone perfusion imaging of the knee using arterial spin labeling MRI. *Magn Reson Med*:1–10 <https://doi.org/10.1002/mrm.28142>
58. Gatehouse PD, Bydder GM (2003) Magnetic resonance imaging of short T2 components in tissue. *Clin Radiol* 58:1–19 <https://doi.org/10.1053/crad.2003.1157>
59. Robson MD, Benjamin M, Gishen P, Bydder GM (2004) Magnetic resonance imaging of the Achilles tendon using ultrashort TE (UTE) pulse sequences. *Clin Radiol* 59:727–735 <https://doi.org/10.1016/j.crad.2003.11.021>
60. Larson PEZ, Han M, Krug R et al (2016) Ultrashort echo time and zero echo time MRI at 7T. *MAGMA* 29:359–370 <https://doi.org/10.1007/s10334-015-0509-0>
61. Juras V, Zbyn S, Pressl C et al (2012) Regional variations of T2* in healthy and pathologic achilles tendon in vivo at 7 Tesla: Preliminary results. *Magn Reson Med* 68:1607–1613 <https://doi.org/10.1002/mrm.24136>
62. Han M, Larson PEZ, Liu J, Krug R (2014) Depiction of achilles tendon microstructure in vivo using high-resolution 3-dimensional ultrashort echo-time magnetic resonance imaging at 7 T. *Invest Radiol* 49:339–345 <https://doi.org/10.1097/RLI.0000000000000025>

63. Juras V, Zbyňň Š, Pressl C et al (2012) Sodium MR imaging of Achilles tendinopathy at 7 T: Preliminary results. *Radiology* 262:199–205 <https://doi.org/10.1148/radiol.111110897>
64. Anz AW, Edison J, Denney TS et al (2020) 3-T MRI mapping is a valid in vivo method of quantitatively evaluating the anterior cruciate ligament: rater reliability and comparison across age. *Skeletal Radiol* 49:443–452 <https://doi.org/10.1007/s00256-019-03301-1>
65. Hager B, Walzer SM, Deligianni X et al (2019) Orientation dependence and decay characteristics of T2* relaxation in the human meniscus studied with 7 Tesla MR microscopy and compared to histology. *Magn Reson Med* 81: 921–933 <https://doi.org/10.1002/mrm.27443>
66. Wang M, Tsang A, Tam V, Chan D, Cao P, Wu EX (2019) Multiparametric MR investigation of proteoglycan diffusivity, T2 relaxation, and concentration in an ex vivo model of intervertebral disc degeneration. *J Magn Reson Imaging* 51:1390–1400 <https://doi.org/10.1002/jmri.26979>
67. Noebauer-Huhmann IM, Juras V, Pfirrmann CWA et al (2012) Sodium MR imaging of the lumbar intervertebral disk at 7 T: Correlation with T2 mapping and modified Pfirrmann score at 3 T - Preliminary results. *Radiology* 265:555–564 <https://doi.org/10.1148/radiol.12111920>
68. Pfirrmann CW, Metzendorf A, Zanetti M, Hodler J, Boos N (2001) Magnetic resonance classification of lumbar intervertebral disc degeneration. *Spine (Phila Pa 1976)* 26:1873–1878 <https://doi.org/10.1097/00007632-200109010-00011>
69. Kerkhof FD, van Leeuwen T, Vereecke EE (2018) The digital human forearm and hand. *J Anat* 233:557–566 <https://doi.org/10.1111/joa.12877>
70. Wang L, Salibi N, Wu Y, Schweitzer ME, Regatte RR (2009) Relaxation times of skeletal muscle metabolites at 7T. *J Magn Reson Imaging* 29:1457–1464 <https://doi.org/10.1002/jmri.21787>
71. Kan HE, Klomp DWJ, Wong CS et al (2010) In vivo 31P MRS detection of an alkaline inorganic phosphate pool with short T1 in human resting skeletal muscle. *NMR Biomed* 23:995–1000 <https://doi.org/10.1002/nbm.1517>
72. Rink K, Berger MC, Korzowski A et al (2015) Nuclear-Overhauser-enhanced MR imaging of 31P-containing metabolites: multipoint-Dixon vs. frequency-selective excitation. *Magn Reson Imaging* 33:1281–1289 <https://doi.org/10.1016/j.mri.2015.07.017>
73. Fiedler GB, Schmid AI, Goluch S et al (2016) Skeletal muscle ATP synthesis and cellular H+ handling measured by localized 31P-MRS during exercise and recovery. *Sci Rep* 6:32037 <https://doi.org/10.1038/srep32037>
74. Korzowski A, Bachert P (2018) High-resolution 31 P echo-planar spectroscopic imaging in vivo at 7T. *Magn Reson Med* 79:1251–1259 <https://doi.org/10.1002/mrm.26785>
75. Kogan F, Haris M, Singh A et al (2014) Method for high-resolution imaging of creatine in vivo using chemical exchange saturation transfer. *Magn Reson Med* 71:164–172 <https://doi.org/10.1002/mrm.24641>
76. Kogan F, Stafford RB, Englund EK et al (2017) Perfusion has no effect on the in vivo CEST effect from Cr (CrCEST) in skeletal muscle. *NMR Biomed* 30: e3673 <https://doi.org/10.1002/nbm.3673>
77. Rösler MB, Nagel AM, Umathum R, Bachert P, Benkhedah N (2016) In vivo observation of quadrupolar splitting in 39K magnetic resonance spectroscopy of human muscle tissue. *NMR Biomed* 29:451–457 <https://doi.org/10.1002/nbm.3476>
78. Heinicke K, Dimitrov IE, Romain N et al (2014) Reproducibility and absolute quantification of muscle glycogen in patients with glycogen storage disease by 13C NMR spectroscopy at 7 tesla. *PLoS One* 9:1–6 <https://doi.org/10.1371/journal.pone.0108706>
79. Towse TF, Childs BT, Sabin SA, Bush EC, Elder CP, Damon BM (2016) Comparison of muscle BOLD responses to arterial occlusion at 3 and 7 Tesla. *Magn Reson Med* 75:1333–1340. <https://doi.org/10.1002/mrm.25562>
80. Food and Drug Administration (2008) Guidance for industry and food and drug administration staff—criteria for significant risk investigations of magnetic resonance diagnostic devices. Silver Spring, MD FDA
81. Gagliardi V, Retico A, Biagi L et al (2018) Subject-specific knee SAR prediction using a degenerate birdcage at 7T. In: MeMeA. IEEE International Symposium on Medical Measurements and Applications, Proceedings, pp 2018–2018
82. Ianni JD, Cao Z, Grissom WA (2018) Machine learning RF shimming: Prediction by iteratively projected ridge regression. *Magn Reson Med* 80: 1871–1881 <https://doi.org/10.1002/mrm.27192>
83. de Vocht F, Stevens T, Glover P, Sunderland A, Gowland P, Kromhout H (2007) Cognitive effects of head-movements in stray fields generated by a 7 Tesla whole-body MRI magnet. *Bioelectromagnetics* 28:247–255 <https://doi.org/10.1002/bem.20311>
84. Hoff MN, McKinney A 4th, Shellock FG et al (2019) Safety considerations of 7-T MRI in clinical practice. *Radiology* 292:509–518 <https://doi.org/10.1148/radiol.2019182742>
85. Cosottini M, Frosini D, Biagi L et al (2014) Short-term side-effects of brain MR examination at 7 T: a single-centre experience. *Eur Radiol* 24:1923–1928 <https://doi.org/10.1007/s00330-014-3177-y>
86. Rietsch SHG, Brunheim S, Orzada S et al (2019) Development and evaluation of a 16-channel receive-only RF coil to improve 7T ultra-high field body MRI with focus on the spine. *Magn Reson Med* 82:796–810 <https://doi.org/10.1002/mrm.27731>
87. Hsu YC, Chu YH, Chern IL, Lattanzi R, Huang TY, Lin FH (2013) Mitigate B1(+) inhomogeneity by nonlinear gradients and RF shimming. *Conf Proc IEEE Eng Med Biol Soc* 2013:1085–1088 <https://doi.org/10.1109/EMBC.2013.6609693>
88. Buonincontri G, Schulte RF, Cosottini M, Tosetti M (2017) Spiral MR fingerprinting at 7 T with simultaneous B1 estimation. *Magn Reson Imaging* 41:1–6 <https://doi.org/10.1016/j.mri.2017.04.003>
89. Gassert FT, Gassert FG, Topping GJ et al (2019) SNR analysis of contrast-enhanced MR imaging for early detection of rheumatoid arthritis. *PLoS One* 14:e0213082 <https://doi.org/10.1371/journal.pone.0213082>
90. Hoogendam JP, Kalleveen IML, de Castro CSA et al (2017) High-resolution T2-weighted cervical cancer imaging: a feasibility study on ultra-high-field 7.0-T MRI with an endorectal monopole antenna. *Eur Radiol* 27:938–945 <https://doi.org/10.1007/s00330-016-4419-y>
91. Lagemaat MW, Scheenen TWJ (2014) Role of high-field MR in studies of localized prostate cancer. *NMR Biomed* 27:67–79 <https://doi.org/10.1002/nbm.2967>
92. Guo X, Gong Y, Wu Z, Yan F, Ding X, Xu X (2020) Renal artery assessment with non-enhanced MR angiography versus digital subtraction angiography: comparison between 1.5 and 3.0 T. *Eur Radiol* 30:1747–1754 <https://doi.org/10.1007/s00330-019-06440-0>

Publisher's Note

Springer Nature remains neutral with regard to jurisdictional claims in published maps and institutional affiliations.

Submit your manuscript to a SpringerOpen[®] journal and benefit from:

- Convenient online submission
- Rigorous peer review
- Open access: articles freely available online
- High visibility within the field
- Retaining the copyright to your article

Submit your next manuscript at ► [springeropen.com](https://www.springeropen.com)